Title

First-principles study of quantum defect candidates in beryllium oxide

Journal

Physical Review B, 106(17)

ISSN

2469-9950

Authors

Chen, Yubi

Turiansky, Mark E

Van de Walle, Chris G

Publication Date

2022-11-01

DOI

10.1103/physrevb.106.174113

First-principles study of quantum defect candidates in beryllium oxide

Yubi Chen and Mark E. Turiansky
Department of Physics, University of California, Santa Barbara, California 93106-9530, USA

Chris G. Van de Walle*
Materials Department, University of California, Santa Barbara, California 93106-5050, USA

Beryllium oxide (BeO) is a promising host for quantum defects because of its ultrawide band gap. We conducted comprehensive first-principles investigations of the native point defects in BeO using density functional theory with a hybrid functional. We found that the beryllium and oxygen vacancies are the most stable defects, whereas other native defects such as interstitials or antisites have high formation energies. We investigate the point defects as candidates for quantum defects by examining spin states and internal optical transitions. The oxygen vacancy (V_{O}^{+}) emerges as a suitable spin qubit or single-photon emitter; we also find its stability can be enhanced by forming a $(V_{\mathrm{O}}{-}\mathrm{Li}_{\mathrm{Be}})^{0}$ complex with a Li acceptor. The $\mathrm{O}_{\mathrm{Be}}^{-}$ antisite also has desirable optical and spin properties. Overall, because of its desirable properties as a host material, BeO could be an excellent host for quantum defects, with V_{O}^{+}, $(V_{\mathrm{O}}-\mathrm{Li}_{\mathrm{Be}})^{0}$, and $\mathrm{O}_{\mathrm{Be}}^{-}$ as prime candidates.

I. INTRODUCTION

Beryllium oxide (BeO) is stable in the wurtzite structure and has a band gap exceeding 10 eV.[1] The material has a high melting temperature, high electrical resistivity, and a high thermal conductivity, which make it useful for a variety of applications such as ceramics and protective coatings.[2,3] Beryllium is also the primary plasma-facing material used in the International Thermonuclear Experimental Reactor (ITER)[4] and is likely covered by its oxide, BeO. Because of its ultrawide band gap, BeO may also be a good host material for quantum defects (qubits or single-photon emitters).[5] For all of these applications, a solid understanding of the prevalence and properties of native point defects is important.

Experimentally, electron spin resonance (ESR) has been used to study point defects in BeO, including the Be vacancy (V_{Be}),[6] the O vacancy V_{O},[7,8] and the Li impurity ($\mathrm{Li}_{\mathrm{Be}}$).[9] Optical absorption and luminescence spectra were also reported.[10] Some first-principles calculations have been performed, but they are incomplete. Wrasse and Baierle[11] performed calculations based on density functional theory (DFT) with the local density approximation (LDA), but they only considered defects in the neutral charge state. Song *et al.*[12] used a semilocal functional in their defect calculations (applying only a correction to the band edges using a hybrid functional), and limited their investigation to the oxygen vacancy (F center). A comprehensive and consistent study of native defects in BeO is thus still lacking.

In this paper we will present results of state-of-the-art first-principles calculations for native point defects in BeO, based on DFT with a hybrid functional. We will focus on the potential to serve as functional defects for quantum information applications. Defects embedded in semiconductors or insulators can make good qubits, because the incorporation in the host lattice provides isolation from one another and from the environment, while still offering access via optical read-out.[13] To be candidates for spin qubits, quantum defects should satisfy a number of criteria:[5] (1) they should have a paramagnetic ground state; (2) the defect states involved in an optical transition should be sufficiently energetically separated from each other, and from the band edges, to avoid thermal excitation; and (3) an optical pumping cycle should exist to initialize the qubit state. The wide band gap of BeO facilitates satisfying (2). Single-photon emitters are another class of quantum defect, which produce photons in a well-defined quantum state, with the photon acting as a qubit. For a single-photon emitter, small electron-phonon coupling is desired. The negatively charged nitrogen-vacancy (NV^{-}) center in diamond is the prototype of point-defect qubits.[14] With a stable triplet (spin-1) ground state, the NV^{-} center has a spin-preserving optical excitation from a highest-occupied defect state to a lowest-unoccupied defect state, which are both deep within the band gap.

Our comprehensive assessment of the atomic and electronic structure of native defects in BeO will show that the oxygen vacancy is the dominant native defect in thermodynamic equilibrium under Be-rich conditions, while the beryllium vacancy is dominant under O-rich conditions. Other defects have high formation energies, but could still be formed by implantation or irradiation. Based on the criteria outlined above, we propose candidates for quantum defects and also evaluate their optical properties. We identify the beryllium vacancy in a neutral charge state (V_{Be}^{0}) as a potential qubit that shares characteristics with the NV center in diamond. However, V_{Be}^{0} has a stronger electron-phonon coupling than the NV center; still, the center could have applications in quantum sensing.[13] Other potential spin qubits or single-photon emitters are $\mathrm{O}_{\mathrm{Be}}^{-}$, V_{O}^{+}, and V_{Be}^{+}, which all have smaller electron-phonon coupling than NV^{-}. We also explored whether forming complexes with impurities can improve or enhance the properties. For V_{Be}, forming a complex with F_{O} lowers the formation energy, but does not yield a better quantum defect. For V_{O}, forming a

complex with Li_{Be} enhances the stability and reduces its electron-phonon coupling.

This paper is arranged as follows. Section II covers the DFT methodology and the theoretical framework for studying defects. Section III shows the results for BeO defect structures and energies, spin properties, and electronic states, and discusses potential quantum defects. Section IV summarizes our results.

II. METHODOLOGY

A. Computational details

Our first-principles calculations are performed using the Vienna Ab initio Simulation Package (VASP 6.2.0).[15,16] Projector augmented wave potentials are used to separate valence and core electrons,[17] employing the VASP-recommended potentials. The valence wavefunctions are expanded in a plane-wave basis with a 400 eV energy cutoff. For the bulk BeO primitive cell, a 9×9×5 Monkhorst-Pack **k**-point mesh is used for integration over the Brillouin zone. Defects are simulated using the supercell approach.[18,19] One defect is generated in a large BeO supercell with 96 atoms, and a single special **k** point $(1/4, 1/4, 1/4)$ is used to sample the Brillouin zone.[20] Convergence tests (using a Gamma-centered 2x2x2 k-point grid) indicated that formation energies are converged to within 0.01 eV at this level of k-point sampling. We also tested convergence as a function of supercell size (going up to 288-atom cells) and found differences in formation energies and Kohn-Sham states of less than 0.05 eV. Spin polarization is explicitly taken into account. The atomic coordinates are relaxed until forces are less than 0.01 eV/Å.

To overcome inaccuracies in the electronic structure associated with local (LDA) or semilocal (GGA) functionals,[21,22] we employ the hybrid functional of Heyd, Scuseria, and Ernzerhof (HSE),[23,24] which enables accurate evaluation of energetics, electronic structure and atomic geometries of bulk properties as well as point defects and impurities.[18] The mixing parameter α describes the extent to which short-range Hartree-Fock exchange replaces PBE exchange in the exchange-correlation functional. We choose $\alpha = 0.405$, which results in a band gap of 11.30 eV. This value agrees well with the experimental value of 10.63 eV[1] after accounting for zero-point renormalization of 0.70 eV.[25] All calculations in this manuscript are performed consistently at the HSE level, including full structural relaxations.

B. Defect formation energy

To evaluate the stability of defects, we calculate their formation energies (E^f). The energy cost to form a defect X in charge state q is[18]

$$E^f[X^q] = E_{\rm tot}[X^q] - E_{\rm tot}[\text{bulk}] - \sum_i n_i\mu_i + qE_{\rm F} + \Delta^q. \tag{1}$$

$E_{\rm tot}[\text{bulk}]$ is the total energy of a bulk supercell, and $E_{\rm tot}[X^q]$ is the total energy of a supercell containing the defect. n_i indicates the number of atoms that are added ($n_i > 0$) or removed ($n_i < 0$) to form the defect, and μ_i is the chemical potential of atomic species i. $E_{\rm F}$ is the Fermi level, i.e., the chemical potential of electrons, and is referenced to the valence-band maximum (VBM). The last term, Δ^q, is a finite-size correction that compensates for the artificial electrostatic interaction between periodic supercells.[26,27] Δ^q is calculated with an HSE dielectric tensor ($\epsilon^{\parallel} = 6.044, \epsilon^{\perp} = 6.664$), which is close to the experimental dielectric constant of 6.7.[28] In equilibrium, the defect concentration is given by $c[X^q] = N_{\rm sites}\exp(-E^f[X^q]/k_BT)$, where $N_{\rm sites}$ is the number of defect sites and T is the temperature.[18] Thus, a defect with a smaller formation energy results in a higher concentration.

The chemical potential of an atomic species, which corresponds to the energy cost of exchanging atoms with a reservoir, is $\mu_i = \mu_{{\rm ref},i} + \Delta\mu_i$, where $\mu_{{\rm ref},i}$ is the reference chemical potential of species i, and $\Delta\mu_i$ captures the abundance of the atomic species in the environment.[18] For Be the reference is the energy of bulk Be metal, and for O the reference is the O_2 molecule. In thermodynamic equilibrium the $\Delta\mu_i$ satisfy

$$\Delta\mu_{\rm Be} + \Delta\mu_{\rm O} = \Delta H_f(\text{BeO}) \ , \tag{2}$$

where $\Delta H_f(\text{BeO})$ is the formation enthalpy of BeO. The HSE-calculated value of $\Delta H_f(\text{BeO})$ is −6.03 eV, in good agreement with the experimental value of −6.32 eV.[2] We assume $\Delta\mu_i \le 0$ to avoid forming elemental phases. $\Delta\mu_{\rm Be} = 0$ corresponds to Be-rich conditions; Eq. (2) then gives $\Delta\mu_{\rm O} = \Delta H_f(\text{BeO})$. O-rich conditions correspond to $\Delta\mu_{\rm O} = 0$, for which $\Delta\mu_{\rm Be} = \Delta H_f(\text{BeO})$. For impurities, we chose chemical potentials to correspond to equilibrium with solubility-limiting phases; we determined these to be Li_2O for Li and BeF_2 for F.

Defect charge-state transition levels $\varepsilon(q/q')$ are defined as the Fermi-level position where the most stable charge state changes from q to q'. They are calculated as[18]

$$\varepsilon(q/q') = \frac{E^f[X^q; E_{\rm F}=0] - E^f[X^{q'}; E_{\rm F}=0]}{q'-q} \ , \tag{3}$$

where $E^f[X^q; E_{\rm F}=0]$ is the formation energy of defect X with charge q when the Fermi level is at the VBM.

C. Modeling of optical transitions

In this paper we will focus on internal transitions, which occur for example when an electron is

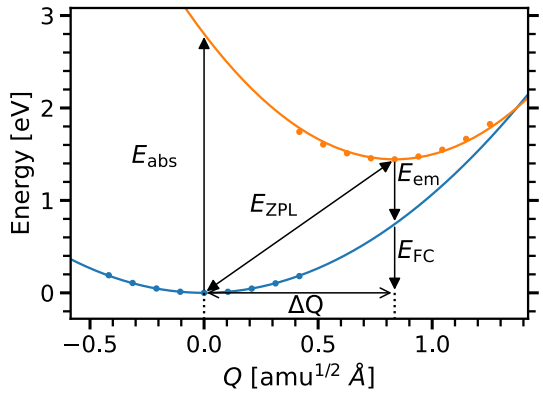

FIG. 1. Configuration-coordinate diagram for the internal transition of V_{Be}^0. The lower (blue) curve corresponds to the ground state of V_{Be}^0, and the upper orange curve to the excited state. Q is the generalized coordinate, and ΔQ indicates the difference between ground-state and excited-state geometries. The dots are calculated data points and the solid curves are parabolic fits. E_{ZPL} is the energy of the zero-phonon line, E_{abs} the absorption energy, E_{em} the emission energy, and E_{FC} the Frank-Condon energy.

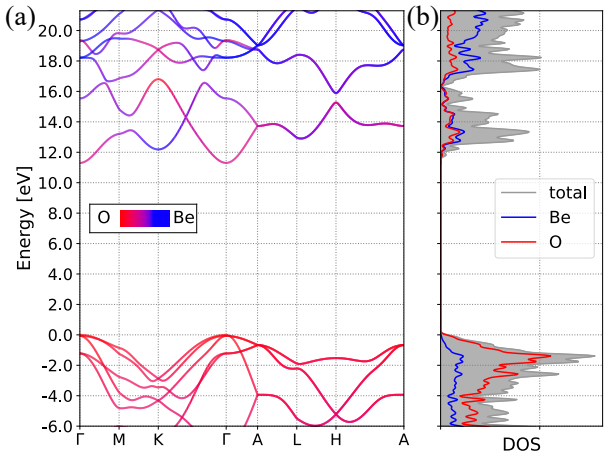

FIG. 2. (a) Band structure and (b) density of states (DOS) for wurtzite BeO. The coloration of the bands indicates the atomic character of the states, according to the color bar. The origin of energy is chosen at the VBM.

lifted from an occupied defect state to an unoccupied state.[13] Excited states are calculated within the Delta-self-consistent-field (ΔSCF) formalism, allowing for full atomic relaxation in a constrained-occupation DFT approach.[29] A symmetry analysis enables us to determine if the transition is dipole allowed. More detailed information about optical properties, in particular about the electron-phonon coupling strength, can be obtained by constructing a configuration coordinate (CC) diagram,[30] which we construct using the nonrad code.[31]

Figure 1 shows the CC diagram for V_{Be}^0 as an example. The horizontal axis is the generalized coordinate Q, which characterizes collective atomic displacements in an one-dimensional approximation by linear interpolation between the geometries of ground and excited states. ΔQ describes the mass-weighted difference between these geometries and is defined as $(\Delta Q)^2 = \sum_i M_i |\mathbf{R}_{e,i} - \mathbf{R}_{g,i}|^2$, where M_i is the mass of atom i, and $\mathbf{R}_{g,i}$ ($\mathbf{R}_{e,i}$) are the atomic coordinates of atom i in the ground (excited) state.[30]

The vertical axis in Fig. 1 is the total energy, and the curve correspond to the ground state and excited state of V_{Be}^0. E_{ZPL} is the zero-phonon line (ZPL) energy, representing the transition where no phonons are involved. The peak of absorption will occur at (or near) the vertical transition for which Q is conserved at the value corresponding to the minimum energy for the ground state ($Q = 0$); the corresponding energy is E_{abs}. For the excited state, the $Q = 0$ geometry corresponds to a configuration that is higher in energy than the minimum energy, and the system will release the extra energy by emitting phonons. Subsequently the defect can return to the ground state by emitting a photon with energy E_{em}; again, the extra energy (referred to as the Franck-Condon energy $E_{FC} = E_{\mathrm{ZPL}} - E_{\mathrm{em}}$) will be released into phonons. The Huang-Rhys[32] (HR) factor $S = \frac{E_{\mathrm{FC}}}{\hbar\Omega_g}$ corresponds to the number of phonons emitted and represents the strength of electron-phonon coupling; Ω_g is the vibrational frequency of the ground state. For efficient optical control and readout of qubits, and for single-photon emitters, it is desirable that a significant portion of the emission occurs in the zero-phonon line. The fraction of the overall intensity that goes into the zero-phonon line can be estimated using $\exp(-S)$.[13] A small Huang-Rhys factor is therefore desirable.

III. RESULTS AND DISCUSSION

A. Bulk properties

BeO assumes the wurtzite crystal structure with point-group symmetry C_{6v} and space-group symmetry $P6_3mc$. The computed lattice parameters of BeO are $a = 2.653$ Å, $c = 4.304$ Å, and $u = 0.3778$, in good agreement with the experimental values, $a = 2.698$ Å, $c = 4.377$ Å (Refs. 33 and 34), and $u = 0.3785$ (Ref. 35).

The BeO band structure and density of states are shown in Fig. 2. The band gap is direct at the Γ point. The VBM is predominantly composed of O p states, with a crystal-field splitting of 67 meV. The conduction-band minimum (CBM) contains similar amounts of Be and O s-state character.

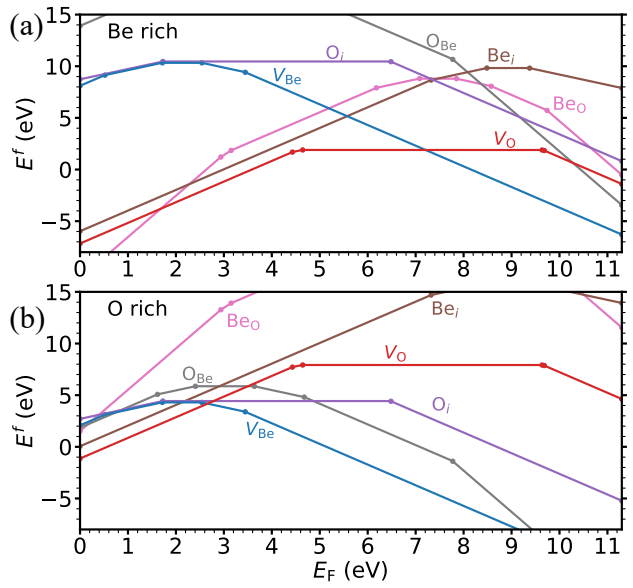

FIG. 3. Formation energy E^f of native defects in BeO as a function of Fermi level E_F under (a) Be-rich and (b) O-rich conditions. Only charge states with the lowest formation energies are shown.

B. Formation energies

1. *Native defects*

The formation energies of the native defects under Be-rich and O-rich conditions are shown in Fig. 3. The corresponding charge-state transition levels are shown in Fig. 4.

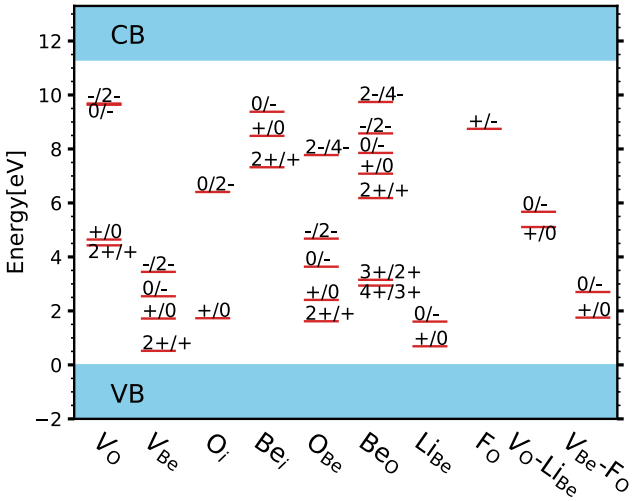

FIG. 4. Charge-state transition levels for point defects, impurities, and complexes in BeO. The valence-band (VB) and conduction-band (CB) energy regions are plotted in blue.

In an actual material, the position of the Fermi level is determined by charge neutrality; i.e., the total charge corresponding to the concentrations of charged defects (and any carriers in the bands, which are absent in the case of an insulator like BeO) needs to be zero. In thermodynamic equilibrium, the concentrations are determined by the formation energies, and the Fermi level will be pinned close to the intersection of the formation energies of the lowest-energy positively charged and negatively charged defects. In the absence of any impurities, Fig. 3 shows that the Fermi level will be pinned far from band edges. Under Be-rich conditions, the O vacancy V_O is the dominant defect, while the Be vacancy V_{Be} is dominant in O-rich conditions. Assuming that V_O^{2+} and V_{Be}^{2-} determine the Fermi-level position, one easily obtains that the formation energy of these relevant native defects would be close to 4.6 eV; in equilibrium, the resulting concentration would then still be less than parts per million even at a growth temperature of 3500 °C.

The impact of impurities will be discussed in Sec. III B 2. Electrically active impurities can shift the Fermi level; it is interesting to note that in BeO the allowed range of Fermi levels is severely restricted. For acceptor doping (which drives the Fermi level down), there is a small region near the VBM (below 0.57 eV) where V_O^{2+} has a negative formation energy, even under the most highly O-rich conditions [Fig. 3(b)], and hence the material would be unstable. For donor doping, the corresponding region is much larger: when the Fermi level is driven above 8.15 eV, the formation energy of V_{Be}^{2-} becomes negative even under the most highly Be-rich conditions [Fig. 3(a)]. This means that (at least under equilibrium conditions) Fermi level positions within 3.15 eV of the CBM will not be attainable.

2. *Impurities and complexes*

Real materials contain impurities, which are either introduced intentionally (as dopants) or unintentionally, during growth or processing. It is not our intent to provide a comprehensive study, but rather to focus on two prototype impurities, one with acceptor character (Li_{Be}), and one with donor character (F_O). The formation energies are shown in Fig. 5. As expected, Li_{Be} is stable mainly in the negative charge state for the majority of Fermi levels, while F_O prefers the positive charge states. The negative charge state of F_O corresponds to a *DX*-like configuration with a large lattice relaxation,[36] but occurs only for Fermi levels for which the material is not thermodynamically stable.

These prevailing charge states determine how the impurities interact with point defects. Specifically, the Li acceptor will tend to bind with oxygen vacancies, which have donor character, and form a V_O–Li_{Be} complex. In the neutral charge state, the complex has a binding energy of 1.47 eV, relative to the V_O^+ and Li_{Be}^-. The F donor will tend to bind with beryllium vacancies, which have acceptor character, and form a V_{Be}–F_O complex. In the negative charge state, this complex has a binding energy

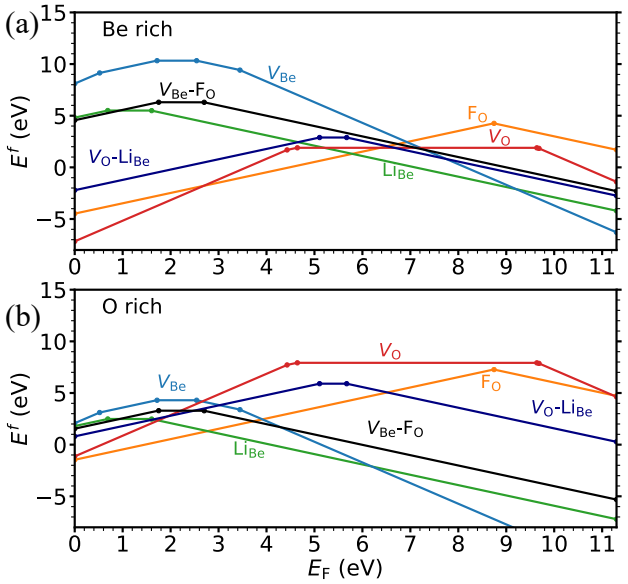

FIG. 5. Formation energy E^f as a function of Fermi level E_F for Li_{Be} and F_O impurities in BeO under (a) Be-rich and (b) O-rich conditions. Also shown are formation energies of the V_O−Li_{Be} and V_{Be}−F_O complexes.

of 2.83 eV, relative to the V_{Be}^{2-} and F_O^+ constituents. The formation of these complexes also shifts the charge-state transition levels (see Fig. 4) and affects the stability of certain charge and spin states. We will return to this issue in Sec. III D 2.

C. Atomic and electronic structure

For a given defect to be useful as a spin qubit, the ground state should possess a non-zero spin. We summarize the ground-state spin of each of the relevant charge states for all native defects, impurities, and complexes in Table I.

We now discuss the defects in more detail. Additional information about atomic and electronic structure is included in Sec. S1 of the Supplemental Material.[37]

1. *Oxygen vacancy*

Each O atom in BeO has four Be nearest neighbors, and each bond contains $\frac{1}{2}$ electron from Be and $\frac{3}{2}$ electrons from O. Removing an O atom creates four dangling bonds on the surrounding Be atoms, to be occupied with two electrons ($\frac{1}{2}$ electron from each Be) in the neutral charge state. In the tetrahedrally bonded crystal environment, the dangling-bond orbitals combine into a symmetric bonding orbital (a_1) and three antibonding orbitals. In the neutral charge state, the two electrons occupy the a_1 orbitals. Giving up one (two) electrons leads to the + (2+) charge state; the corresponding occupation

TABLE I. Ground-state spin for point defects, impurities, and complexes in BeO. Parentheses indicate charge states that are metastable. Spin states for which an internal optical transition can occur are marked in bold. The † symbol points out charge states that lie outside the attainable Fermi-level range (0.57–8.15 eV, see Sec. III B 1).

	defect charge								
	4+	3+	2+	+	0	−	2−	3−	4−
V_O	—	—	0	**1/2**	**0**	**1/2**†	**0**†	—	—
V_{Be}	—	—	2†	**3/2**	**1**	**1/2**	0	—	—
O_i	—	—	—	**1/2**	0	(**1/2**)	0	—	—
Be_i	—	—	0	1/2	**0**†	**1/2**†	—	—	—
O_{Be}	—	—	0	**1/2**	**0**	**1/2**	0	(**1/2**)	0
Be_O	0	**1/2**	**0**	**1/2**	**0**	**3/2**	**1**†	(**1/2**)†	0†
Li_{Be}	—	—	—	0	1/2	0	—	—	—
F_O	—	—	—	0	(1/2)	**0**†	—	—	—
V_O−Li_{Be}	—	—	—	**0**	**1/2**	**0**	—	—	—
V_{Be}−F_O	—	—	—	**1**	**1/2**	0	—	—	—

of the Kohn-Sham (KS) states is shown in Fig. S2 of the Supplemental Material.[37]

The oxygen vacancy can also accept electrons in the antibonding states. In many oxides (e.g., ZnO[38]), these antibonding orbitals are well above the CBM and hence they cannot accept electrons, but the gap of BeO is sufficiently wide to accommodate the antibonding states (see Fig. S2), resulting in negative charge states becoming stable. Details about the atomic geometry in the various charge states are included in Fig. S1 of the Supplemental Material.[37]

Our calculated ground-state spin and level structure for V_O^0 agree with Ref. 7. V_O^+ has been experimentally observed as well, in neutron irradiated samples.[39]

2. *Beryllium vacancy*

The removal of a Be atom in BeO leaves six electrons to be accommodated in defect states in the neutral charge state. V_{Be} can therefore accept two more electrons, giving rise to − and 2− charge states (see Fig. 3). Positive charge states can also be stabilized for Fermi levels close to the VBM. The oxygen dangling bonds combine into a symmetric bonding orbital (a_1), which overlaps with the valence band, and three antibonding orbitals. Oxygen orbitals are much more spatially localized than Be orbitals, and hence the bonding-antibonding splitting is much smaller than in the case of the oxygen vacancy, and all of the KS states are located in the vicinity of the VBM (Fig. 6). The KS states are evaluated at the single, special k-point, which provides a good approximation to the dilute limit.[18] Details about the atomic geometry in the various charge states are included in Fig. S3 of the Supplemental Material.[37]

The spins of V_{Be}^- and V_{Be}^0 are consistent with the ESR results of Ref. 6. V_{Be}^- has seven electrons and a doublet ground state. The unoccupied KS state is local-

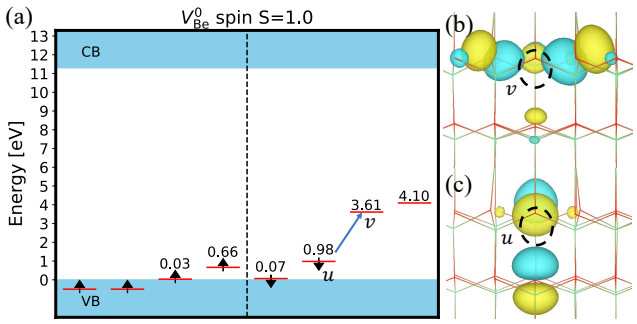

FIG. 6. (a) Kohn-Sham states of V_{Be}^0 (red segments); spin-up states are shown in the left panel, spin-down states in the right panel. The valence-band (VB) and conduction-band (CB) energy regions are plotted in blue. Electrons occupying defect states are indicated with black arrows. (b)-(c) Isosurfaces for the real part of the wave function for (b) the lowest unoccupied (v) KS state and (c) the highest occupied (u) KS state. The isosurface corresponds to 5% of the maximal value and blue and yellow indicate opposite signs. Dashed circles point out the defect positions.

ized around one in-plane nearest-neighbor atom. Maffeo and Hervé[6] reported hyperfine parameters for a ^{9}Be nucleus based on electron-nuclear double resonance (ENDOR) measurements on V_{Be}^-. Our calculated value for the isotropic hyperfine parameter, 2.5 MHz, is in good agreement with the value of 3.33 MHz reported in Ref. 6. The ground-state spin of V_{Be}^0 is a triplet, similar to the case of the prototypical quantum defect—the NV center in diamond. We will therefore pay particular attention to this defect and discuss it in detail in Sec. III D 1.

3. *Oxygen interstitial*

The oxygen interstitial O_i can be stable in +, 0, and 2− charge states (Fig. 3); the − charge state is always higher in energy than 0 or 2−. The oxygen interstitial has fairly high formation energy and is never the lowest-energy native defect in thermodynamic equilibrium. The neutral and 2− charge states both have zero spins; the + charge state, which has spin-1/2, could be a qubit candidate, but is unlikely to occur since it requires the Fermi level to be very low in the band gap.

4. *Beryllium interstitial*

Not surprisingly for a divalent interstitial, the preferred charge state of the beryllium interstitial Be_i is 2+ (Fig. 3). Be_i^{2+} and Be_i^0 have zero-spin ground states and are therefore not candidates for spin qubits. Be_i^+ has spin 1/2 but no suitable internal transitions. Be_i^- could be a spin-qubit candidate but is unlikely to occur since it is stable only when the Fermi level is high in the gap.

5. *Oxygen antisite*

Oxygen antisites O_{Be} can occur in charge states ranging from 2+ to 4−. In the +, − and 3− charge states, the ground-state spin is 1/2. While the formation energy is high, these defects could potentially be formed by ion implantation or irradiation, and the range of Fermi-level positions for which the − charge state is stable (Fig. 3) indicates it is more likely to occur.

6. *Beryllium antisite*

Beryllium antisites Be_O can occur in charge states ranging from 4+ to 4−. Under O-rich conditions, Be_O^{2+} are the most stable defects for Fermi-level positions close to the VBM, but these are unlikely to occur. Otherwise, Be_O has high formation energy. It could still be formed under non-equilibrium conditions, but the presence of multiple possible charge states would render it difficult to stabilize suitable spin states. In fact, the 4+ and 2+ charge states that are stable over the largest range of Fermi levels have spin zero and are therefore not candidates for spin qubits.

D. Quantum defect candidates

1. *Beryllium vacancy example*

We illustrate our procedure for identifying candidate quantum defects with the example of V_{Be}^0. The KS states of V_{Be}^0 are shown in Fig. 6. In this diagram, the KS states of the defect are positioned relative to the bulk VBM and CBM by taking the potential alignment between bulk and defect supercells into account.[26,27]

The two unoccupied KS states in V_{Be}^0 are in the same spin channel, resulting in a triplet (spin-1) ground state, similar to the prototypical quantum defect—the NV center in diamond. The two holes localize around two in-plane nearest-neighbor atoms of V_{Be}^0, which move radially outward from the vacancy; the symmetry is C_{1h} (mirror symmetry). An internal transition [indicated by the blue arrow in Fig. 6(a)] can occur in which an electron is excited from state u at 0.98 eV to state v at 3.61 eV. Both u and v correspond to the a' irreducible representation (the identity representation) of C_{1h}; a symmetry analysis indicates that the transition is dipole-allowed. The wavefunctions of the KS states are shown in Figs. 6(b) and (c). The many-body ground and excited states are both $^3A''$ triplet states.

The energy difference between the u and v states, 2.63 eV, provides an estimate for the peak energy in optical absorption. This value is indeed close to the value $E_{abs} = 2.80$ eV (see the CC diagram in Fig. 1) for the vertical transition obtained from total energy calculations. Values for this absorption energy as well as for the ZPL and emission energies are included in Table II. The table

also lists values for the HR factor S. Unfortunately, the HR factor for V_{Be}^{0} is very large ($S = 7.88$), indicating that this defect will not be an efficient emitter.

2. *Candidates for spin qubits*

We can apply this type of analysis to other defects that were identified as potential spin qubits in Table I, based on being stable in nonzero spin states and having an internal optical transition. The results for the most promising candidates, as discussed in Sec. III C are summarized in Table II. Relevant CC diagrams are included in Sec. S2 of the Supplemental Material.[37]

TABLE II. Parameters characterizing the optical transitions for quantum defect candidates in BeO. The symmetry group ("sym") and relevant transition are also listed.

	Spin	E_{ZPL}	E_{abs}	E_{em}	E_{FC}	S	sym	transition
V_{O}^{+}	1/2	5.45	5.79	5.20	0.25	3.29	C_{3v}	$A_1 \rightarrow A_1$
V_{O}^{0}	0	5.09	5.92	4.22	0.87	15.42	C_{3v}	$A_1 \rightarrow A_1$
$(V_{\mathrm{O}}-\mathrm{Li}_{\mathrm{Be}})^{0}$	1/2	5.20	5.57	4.96	0.24	3.15	C_{1h}	$A' \rightarrow A'$
V_{Be}^{+}	3/2	1.83	2.38	1.58	0.25	3.06	C_{3v}	$A_2 \rightarrow A_2$
V_{Be}^{0}	1	1.44	2.80	0.70	0.74	7.88	C_{1h}	$A'' \rightarrow A''$
$(V_{\mathrm{Be}}-\mathrm{F}_{\mathrm{O}})^{+}$	1	1.83	3.06	1.07	0.76	8.18	C_1	$A \rightarrow A$
$(V_{\mathrm{Be}}-\mathrm{F}_{\mathrm{O}})^{0}$	1/2	1.70	3.94	0.42	1.29	13.64	C_1	$A \rightarrow A$
$\mathrm{O}_{\mathrm{Be}}^{-}$	1/2	2.95	3.41	2.73	0.22	2.41	C_1	$A \rightarrow A$

As discussed in Sec. II C, a low Huang-Rhys factor is desirable for single-photon emitters and for efficient control of qubits. For reference, the prototype quantum defect, the NV^{-} center, has a HR factor $S = 3.7$. As Table II shows, $\mathrm{O}_{\mathrm{Be}}^{-}$, V_{O}^{+}, $(V_{\mathrm{O}}-\mathrm{Li}_{\mathrm{Be}})^{0}$, and V_{Be}^{+} have relatively small HR factors.

V_{O}^{+} is of particular interest because it is expected to form quite easily and has been experimentally observed.[39] It has spin 1/2, an optical transition in the UV-C range, and a relatively small HR factor. However, as seen in Fig. 3, it is stable only over a narrow range of Fermi levels (a result that was verified by explicitly checking convergence with respect to k-point sampling). It is interesting to explore whether complex formation could enhance the stability of a desired spin state. Indeed, by forming a complex with $\mathrm{Li}_{\mathrm{Be}}^{-}$, we obtain a $(V_{\mathrm{O}}-\mathrm{Li}_{\mathrm{Be}})^{0}$ complex with physical properties that are similar to those of V_{O}^{+}: the spin state is spin-1/2 (Table I), the ZPL energy is 5.20 eV (compared to 5.45 eV, Table II), and the internal transition is physically the same. However, the $(V_{\mathrm{O}}-\mathrm{Li}_{\mathrm{Be}})^{0}$ complex is stable over a wider range of Fermi levels (from 5.11 to 5.67 eV) (Fig. 4), and it features a slightly smaller HR factor (3.15 instead of 3.29, Table II). Intentional doping with Li, which acts as an acceptor and drives the Fermi level down, will promote the formation of V_{O} for charge compensation (Fig. 5), and the large binding energy (1.47 eV) of the $(V_{\mathrm{O}}-\mathrm{Li}_{\mathrm{Be}})^{0}$ renders its formation feasible.

We also checked whether complex formation with a donor, $\mathrm{F}_{\mathrm{O}}^{+}$, might improve the properties of V_{Be}^{0}, particularly its very large HR factor. Both V_{Be}^{0} and $(V_{\mathrm{Be}}-\mathrm{F}_{\mathrm{O}})^{+}$ have spin 1 (Table I), similar to the NV^{-} center in diamond. The ZPL energy is 1.83 eV (Table II), compared to 1.44 eV for V_{Be}^{0}, with similar symmetry properties for the internal transition. Unfortunately, the HR factor is not improved, and is even larger ($S = 8.18$) than for V_{Be}^{0} (Table II). Also, stabilizing the complex in the + charge state requires Fermi levels quite close to the VBM (Fig. 4), which may be hard to achieve. We therefore also explored the neutral charge state, which can be stabilized in roughly the same range of Fermi levels as V_{Be}^{0} (Fig. 4). However, the HR factor ($S = 13.64$) is even larger in this case.

Finally, Table II includes $\mathrm{O}_{\mathrm{Be}}^{-}$, which has the smallest HR factor ($S = 2.41$) of all the defects considered here. It also has a ZPL energy (2.95 eV) that is just within the visible spectrum. As noted in Sec. III C 5, its formation energy is relatively high, but it could be formed by implantation or irradiation.

IV. SUMMARY AND CONCLUSIONS

Using first-principles calculations with a hybrid functional, we have performed a comprehensive study of native point defects in BeO. We found that, in equilibrium and in the absence of impurities, vacancies will be dominant, but the native defects all have high formation energies and would be present in low concentrations. We therefore suggest that in actual materials the Fermi-level position and defect concentrations are determined by unintentionally incorporated impurities.

Vacancies and vacancy-related complexes would still be the dominant defects, and our analysis of internal optical transitions (Table II) indicates that oxygen vacancies may strongly absorb in the UV, and could therefore be detrimental for optical coatings. V_{O} or related complexes could also lead to optical absorption in the deep UV by allowing holes to be excited to the VB or electrons into the CB. As for V_{Be} or related complexes, internal transitions tend to be at lower energies (in the visible range of the spectrum), and the position of the defect levels relatively close to the VB (Fig. 4) indicates that no hole excitation will occur, and electron excitation would take place only at energies exceeding 8 eV (corresponding to the vacuum UV region).

The results for native defects were used to discuss potential quantum defects. Interesting candidates were investigated by analyzing internal optical transitions and constructing CC diagrams. We identified V_{O}^{+}, V_{Be}^{+}, and V_{Be}^{0} as candidates for spin qubits. V_{O}^{+} is of special interest because it has already been experimentally observed[39] and it has a relatively small HR factor. However, the range of Fermi levels over which it is stable is very small. We propose that forming a $(V_{\mathrm{O}}-\mathrm{Li}_{\mathrm{Be}})^{0}$ complex will extend this range, leading to higher stability while main-

taining the desirable spin and optical properties. A similar investigation of complex formation in the case of V_{Be}^{0}, leading to a (V_{Be}−$\mathrm{F_O}$), did not yield the hoped-for improvement. Finally, the antisite defect $\mathrm{O}_{\mathrm{Be}}^{-}$ was found to have suitable optical transitions and a small HR factor. Overall, because of its wide band gap and stability, BeO could be an excellent host for quantum defects, with V_{O}^{+}, $(V_{\mathrm{O}} - \mathrm{Li}_{\mathrm{Be}})^{0}$ and $\mathrm{O}_{\mathrm{Be}}^{-}$ as prime candidates.

ACKNOWLEDGMENTS

Y.C. was supported by the U.S. Department of Energy, Office of Science, National Quantum Information Science Research Centers, Co-design Center for Quantum Advantage (C2QA) under contract number DE-SC0012704. M.E.T. and C.G.VdW. were supported by the National Science Foundation (NSF) through Enabling Quantum Leap: Convergent Accelerated Discovery Foundries for Quantum Materials Science, Engineering and Information (Q-AMASE-i) award number DMR-1906325. Computing resources were provided by the National Energy Research Scientific Computing Center (NERSC), a U.S. Department of Energy Office of Science User Facility located at Lawrence Berkeley National Laboratory, operated under Contract No. DE-AC02-05CH11231.

* vandewalle@mrl.ucsb.edu

[1] D. Roessler, W. Walker, and E. Loh, J. Phys. Chem. Solids **30**, 157 (1969).
[2] D. R. Lide, *CRC Handbook of Chemistry and Physics*, Vol. 85 (CRC Press, 2016).
[3] V. S. Kiiko, A. V. Pavlov, and V. A. Bykov, Refract. Ind. Ceram. **59**, 616 (2019).
[4] L. Ferry, F. Virot, Y. Ferro, D. Matveev, C. Linsmeier, and M. Barrachin, J. Nucl. Mater. **524**, 323 (2019).
[5] J. R. Weber, W. F. Koehl, J. B. Varley, A. Janotti, B. B. Buckley, C. G. Van de Walle, and D. D. Awschalom, Proc. Natl. Acad. Sci. **107**, 8513 (2010).
[6] B. Maffeo and A. Hervé, Phys. Rev. B **13**, 1940 (1976).
[7] S. V. Gorbunov, A. V. Kruzhalov, and M. J. Springis, Phys. Status Solidi B **141**, 293 (1987).
[8] A. Kruzhalov, V. Ivanov, K. Bautin, O. Ryabukhin, A. Korotaev, and V. Pustovarov, Nucl. Instrum. Methods Phys. Res., Sect. A **486**, 325 (2002).
[9] R. C. Duvarney and A. K. Garrison, Phys. Status Solidi A **42**, 609 (1977).
[10] I. Ogorodnikov and A. Kruzhalov, in *Materials Science Forum*, Vol. 239 (Trans Tech Publ, 1997) pp. 51–56.
[11] E. Wrasse and R. Baierle, Phys. Procedia **28**, 79 (2012).
[12] J. Song, T. Liu, C. Shi, R. Sun, and K. Wu, Mod. Phys. Lett. B **35**, 2150148 (2020).
[13] C. E. Dreyer, A. Alkauskas, J. L. Lyons, A. Janotti, and C. G. Van de Walle, Annu. Rev. Mater. Res. **48**, 1 (2018).
[14] P. Neumann, N. Mizuochi, F. Rempp, P. Hemmer, H. Watanabe, S. Yamasaki, V. Jacques, T. Gaebel, F. Jelezko, and J. Wrachtrup, Science **320**, 1326 (2008).
[15] G. Kresse and J. Furthmüller, Phys. Rev. B **54**, 11169 (1996).
[16] G. Kresse and J. Furthmüller, Comput. Mater. Sci. **6**, 15 (1996).
[17] P. E. Blöchl, Phys. Rev. B **50**, 17953 (1994).
[18] C. Freysoldt, B. Grabowski, T. Hickel, J. Neugebauer, G. Kresse, A. Janotti, and C. G. Van de Walle, Rev. Mod. Phys. **86**, 253 (2014).
[19] C. G. Van de Walle and J. Neugebauer, J. Appl. Phys. **95**, 3851 (2004).
[20] H. J. Monkhorst and J. D. Pack, Phys. Rev. B **13**, 5188 (1976).
[21] L. J. Sham and M. Schlüter, Phys. Rev. Lett. **51**, 1888 (1983).
[22] R. W. Godby, M. Schlüter, and L. J. Sham, Phys. Rev. Lett. **56**, 2415 (1986).
[23] J. Heyd, G. E. Scuseria, and M. Ernzerhof, J. Chem. Phys. **118**, 8207 (2003).
[24] J. Heyd, G. E. Scuseria, and M. Ernzerhof, J. Chem. Phys. **124**, 219906 (2006).
[25] A. Miglio, V. Brousseau-Couture, E. Godbout, G. Antonius, Y.-H. Chan, S. G. Louie, M. Côté, M. Giantomassi, and X. Gonze, npj Comput. Mater. **6**, 1 (2020).
[26] C. Freysoldt, J. Neugebauer, and C. G. Van de Walle, Phys. Rev. Lett. **102**, 016402 (2009).
[27] C. Freysoldt, J. Neugebauer, and C. G. Van de Walle, Phys. Status Solidi B **248**, 1067 (2011).
[28] G. Wypych, Handbook of Fillers (Fourth Edition), Chem. Tec. Publishing , 13 (2016).
[29] R. O. Jones and O. Gunnarsson, Rev. Mod. Phys. **61**, 689 (1989).
[30] A. Alkauskas, Q. Yan, and C. G. Van de Walle, Phys. Rev. B **90**, 075202 (2014).
[31] M. E. Turiansky, A. Alkauskas, M. Engel, G. Kresse, D. Wickramaratne, J.-X. Shen, C. E. Dreyer, and C. G. Van de Walle, Comput. Phys. Commun. **267**, 108056 (2021).
[32] K. Huang and A. Rhys, Proc. Royal Soc. **204**, 406 (1950).
[33] D. K. Smith, H. W. Newkirk, and J. S. Kahn, J. Electrochem. Soc. **111**, 78 (1964).
[34] R. M. Hazen and L. W. Finger, J. Appl. Phys. **59**, 3728 (1986).
[35] P. Lawaetz, Phys. Rev. B **5**, 4039 (1972).
[36] D. J. Chadi and K.-J. Chang, Phys. Rev. Lett. **61**, 873 (1988).
[37] See Supplemental Material at [URL will be inserted by publisher] for details about atomic and electronic structure of defects, and CC diagrams for optical transitions.
[38] A. Janotti and C. G. Van de Walle, Phys. Rev. B **76**, 165202 (2007).
[39] R. C. DuVarney, A. K. Garrison, and R. H. Thorland, Phys. Rev. **188**, 657 (1969).